Regular Article

Mathematical modeling and analytical examination of peristaltic transport in flow of Rabinowitsch fluid with Darcy's law: two-dimensional curved plane geometry

Wei-Mao Qian[1], Arshad Riaz[2], Katta Ramesh[3], Sami Ullah Khan[4], M. Ijaz Khan[5,a], Ronnason Chinram[6], and M. Kbiri Alaoui[7]

[1] School of Continuing Equation, Huzhou Vocational & Technical College, Huzhou 313000, P. R. China
[2] Department of Mathematics, Division of Science and Technology, University of Education, Lahore 54770, Pakistan
[3] Department of Mathematics, Symbiosis Institute of Technology, Symbiosis International (Deemed University), Pune 412115, India
[4] Department of Mathematics, COMSATS University Islamabad, Sahiwal 57000, Pakistan
[5] Department of Mathematics and Statistics, Riphah International University I-14, Islamabad 44000, Pakistan
[6] Division of Computational Science, Faculty of Science, Prince of Songkla University, Hat Yai, Songkhla 90110, Thailand
[7] Department of Mathematics, College of Sciences, King Khalid University, Abha 61413, Saudi Arabia

Abstract In this paper, the authors presented the effects of space voids and electrical conductivity on the flow of a pseudoplastic (Rabinowitsch) fluid analyzed in a curved two-dimensional plane geometry. The walls of the channel are considered to develop the peristaltic waves along its length. The problem is manipulated under the observations of long wavelength and low Reynolds number approximations. The motion is assumed to be steady by transforming it in a wave frame traveling with the speed of wave. Analytical hybrid perturbation techniques have been incorporated to handle the complicated coupled differential equations. It is found that the results are well in agreement with the existing literature as a special case, evocating the validity of the study. Expressions of velocity, pressure gradient, and stream function have been invoked graphically. It is concluded from the results that porous medium and magnetic field suggest opposite variations of velocity and trapping circulating contours are stretching with magnetic field and contracting with increasing voids.

1 Introduction

The biological fluid flows can be generated by continual wavelike rhythmic structures of biological vessels like ureter, intestines, stomach, esophagus, and blood vessels (capillaries, veins, arteries, etc.). These rhythmic structures of smooth muscles are known as the peristaltic phenomenon. This phenomenon may be used in various applications in the physiological systems. For instance, transport of ovum and spermatozoa, fluid motion in uterine, chyme flow in the gastrointestinal tract, motion of food in the esophagus, and motion of urine. These are internal mechanisms of peristaltic phenomenon. Nowadays, external mechanisms of peristalsis exist such as motion of earthworms, finger and roller pumps operate on this mechanism, and micro and nanorobots also use the peristaltic mechanism. Utilizing these concepts, many researchers have studied many problems with peristalsis in the symmetric and asym-

metric channels, which seems unrealistic, because most of the physiological and industrial systems are in curved structures. The concept of curvature in the peristalsis is investigated in only few studies. Riaz et al. [1] have investigated the electromagnetism and permeability measures in Jeffrey fluid through eccentric annuli executing peristaltic porous confines. They have produced the results that pumping rate is enhanced by magnetic field but reduced by porosity factors. Noreen [2] studied the effects of induced MHD on the peristaltic propulsion of viscous fluid in a curved configuration. In this study, the author has proved the symmetry of velocity profiles disturbs in the presence of curvature effects. Riaz et al. [3] achieved exact solutions for multiphase nonlinear fluid expressing peristaltic pumping characteristics in an annulus comprising complaint walls and magnetism is also taken into consideration. It is revealed that imposed magnetic field suppresses the fluid and particle motion. Zeeshan et al. [4] have used curved configuration to study the viscous particulate-fluid suspension in a peristaltic transport. Their observation clears that the concentration of fluid rises with

the curvature parameter. Srinivas and Kothandapani [5] have published the porosity and magnetic effects on thermal and mass transfer analysis of wave type transport including compliant boundaries. Maraj et al. [6] have given the homotopy perturbation solutions for the motion of Williamson fluid under the curved peristalsis. In this study, it is noticed that mixed behavior is noticed for the velocity with the curvature parameter. Akbar and Butt [7] have described the peristaltic nanofluid propulsion in through curved walls, and studied the pressure gradient and velocity variations under the influence of curvature parameter. Some more relevant cases may be observed through various references (see [8–10]) and the references therein.

The study of magnetic field in fluid flow systems attracted many researchers due to its wide range of applications in industry and engineering. This study represents the interaction between the fluid flow and applied magnetic field. The applications include targeted drug delivery, imaging contrast enhancement, nanoparticle manipulation, and laser beam scanning. In view of many applications of magnetohyrodynamics, many researchers have started their research in fluid flows with magnetic field effects. Stiller et al. [11] have presented a review on the recent numerical and experimental investigations of the flow driven by rotating and traveling magnetic fields. Sucharitha et al. [12] have discussed the effect of MHD on the motion of Jeffrey fluid driven by tapered peristalsis. Meenakumari et al. [13] have used a numerical technique named RK. Fehlberg-based shooting technique to discuss the effects of inclined magnetic field on the unsteady motion of Williamson nanofluid over a stretching surface. Samrat et al. [14] have investigated the MHD flow over the paraboloid of revolution. Trivedi and Ansari [15] have performed the analytical study on the Casson nanofluid flow past a linear stretching sheet with inclined magnetic field. Nowadays, the field of biomagnetic fluid dynamics is emerging area of interest in living creatures. In general, biological cells and molecules are considered as biomagnetic materials. The use of magnetic field in the biomedicine can be captured in many ways, such as passage sealers, magnetic hyperthermia, drug delivery, imaging contrast enhancement, and nanoparticle manipulations in biomedical engineering. It is also observed from many studies that the flow patterns rapidly change under the applied magnetic field [16–18]. Narla et al. [19] have provided the detailed examination on the flow variables such as streamlines, pressure rise, and pressure gradient for the flow of an MHD viscoelastic fluid in a peristaltic curved configuration. Ali et al. [20] applied Generalized Differential Quadrature Method (GDQM) to suggest a numerical simulation of peristaltic Flow with changing electrical conductivity and Joule dissipation effects along with MHD. Amanullah et al. [21] have proposed the numerical magnetic field features for Carreau fluid flow numerically through an isothermal sphere.

Porous medium has many applications in engineering and industry, and it has also many applications in biomedicine and bioengineering. Generally, a porous

medium is material with some pores. These pores appear in many biological systems, such as central nervous system, brain aneurysm, drug delivery, tissue replacement, and computational biology. There is a vast study present in literature in the presence of porous medium (for instance, [22–24]), but very few cases have been discussed the effect of porous medium under the peristaltic curved boundaries. Hayat et al. [25] have considered Ellis fluid to investigate the flow in curved peristaltic configuration under the effects of porous medium. The key observation of this study is the velocity enhances with the Darcy number. Mohammadein and Abu-Nab [26] have discussed the motion of Newtonian fluid in a curved geometry under the peristalsis and porous medium with the vapour bubble. From this study, the velocity deduction is observed with permeability. Vajravelu et al. [27] have provided the pumping type passage of Phan–Thien–Tanner fluid by taking porous medium. More literature on porous medium can be found in [28–30].

From the last few decades, the investigation of non-Newtonian materials has received much attention to the investigators in fluid dynamics. Rabinowitsch fluid is one of the non-Newtonian fluids (class of shear thinning liquids). This fluid model perfectly describes the diverse fluid models such as Newtonian, Dilatant, and pseudoplastic fluid in the limiting cases of the Rabinowitsch model. Some of the examples of Rabinowitsch model are blood, whipped cream, and ketchup. Based on these facts in mind, many investigators have focused in the direction of Rabinowitsch fluid flow model. Akbar and Butt [31] have discussed the motion of a Rabinowitsch fluid in the presence of metachronal wave of cilia with the exact solutions. Vaidya et al. [32] have provided the semi-analytical solutions with the help of perturbation technique for the flow of Rabinowitsch fluid under the influence of peristalsis. In this study, the authors have provided the results for the limiting cases such as Newtonian, pseudoplastic, dilatant, and fluid models. In another study, Vaidya et al. [33] have considered the same fluid model with the variable liquid and wall properties. Sadaf and Nadeem [34] have discussed the transport of a Rabinowitsch fluid under the effects of peristalsis and porous medium. Vaidya et al. [35] have focused to study the non-uniform effects of peristalsis on the motion of a Rabinowitsch liquid in the presence of wall properties. Maraj and Nadeem [36] have studied the propulsion of Rabinowitsch liquid under the considerations of peristalsis and curved configuration. Few more studies can be seen in the direction of Rabinowitsch liquid flow model in the references [37–40] and the references therein.

To the best of author's information, no study releases the effects of magnetic field and porous medium effects on rabinowitsch model in a curved channel with a hybrid analytical technique. This study composes the peristaltic flow of Rabinowitsch model executing peristaltic waves through a curved porous channel magnetized by applied normal magnetic field. This study may be helpful in electrical conductions of many industrial for dilatant and pseudoplastic fluids and clinical issues
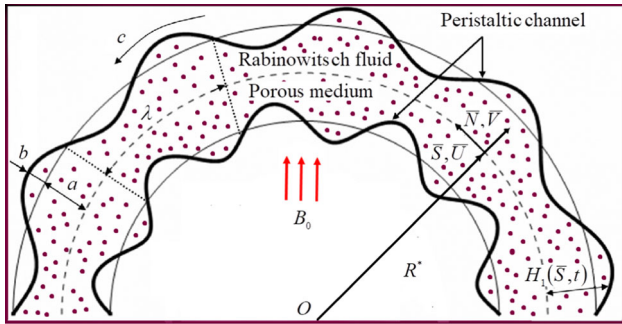
Fig. 1 Physical structure of the problem

for blood flows. The mathematical modeling has been completed by introducing the concept of low Reynolds number and long waves traveling axially. The equations of motion have been explored using wave frame to evaluate the steady incompressible flow. The obtained coupled partial differential equations are handled by two combined analytical perturbation techniques. The expressions of velocity, pressure gradient, and trapping have been dealt through graphical aspect under the variation of physically appearing parameters.

2 Mathematical modeling

Assume a curved channel whose width is $2a$ which is loaded with Rabinowitsch liquid. The radius and center of curvature of the circle, where the channel is wound, are represented by R^* and O, separately. There is a rearrange graph of the stream geometry in Fig. 1. We utilize a curvilinear arrange framework $(\overline{N}, \overline{S}, \overline{Z})$ to inspect the stream in which $\overline{N}$ is coordinated toward the outspread course, $\overline{S}$ is toward the flow line, and vertical way $\overline{Z}$ is the representative.

The Cartesian frame of reference is set at the origin O. It is related with curvilinear facilitate framework as per these changes

$$
\left.
\begin{array}{l}
X' = \left(R^* + \overline{N}\right)\cos\left(\frac{\overline{S}}{R^*}\right) \\[2mm]
Y' = \left(R^* + \overline{N}\right)\sin\left(\frac{\overline{S}}{R^*}\right)
\end{array}
\right\}. \tag{1}
$$

The upper wall equation in (X, Y) system is

$$
X'^2 + Y'^2 = \left((R^* + a) \right.
$$
$$
\left. + b\sin\left(\frac{2\pi}{\lambda}\left(R^*\tan^{-1}\left(\frac{Y'}{X'}\right) - c\bar{t}\right)\right)\right)^2. \tag{2}
$$

Putting Eq. (1) in Eq. (2), we arrive at

$$
\overline{R} = a + b\cos\left(\frac{2\pi}{\lambda}(\overline{S} - c\bar{t})\right). \tag{3}
$$

Supplanting the left-hand side of Eq. (3) by H_1, the condition becomes

$$
H_1(\overline{S}, \bar{t}) = a + b\cos\left(\frac{2\pi}{\lambda}(\overline{S} - c\bar{t})\right), \quad \text{(upper wall)}, \tag{4}
$$

where λ, b, and $\bar{t}$ are the wavelength, amplitude, and the time, separately. In the similar manner, the lower wall equation is

$$
H_2(\overline{S}, \bar{t}) = -a - b\cos\left(\frac{2\pi}{\lambda}(\overline{S} - c\bar{t})\right), \quad \text{(Lower wall)}. \tag{5}
$$

Additionally, the magnetic field $\overline{\mathbf{B}} = (0, B_0)$ is applied orthogonally to the flow direction (radial) and the surfaces of geometry are assumed to be porous with voids in the layers. The MHD is playing a role of body force on the motion of the fluid whose term $\overline{\mathbf{J}} \times \overline{\mathbf{B}}$ is inserted in the momentum equation through Maxwell's equations and the factor of porosity is also included through Darcy's law. The governing equations in component form for the present study have been described below [31–36]

$$
\frac{\partial}{\partial \overline{N}}\left((\overline{N} + R^*)\,\overline{V}\right) + R^*\frac{\partial \overline{U}}{\partial \overline{S}} = 0, \tag{6}
$$

$$
\rho\left[\frac{\partial \overline{V}}{\partial \overline{t}} + \overline{V}\frac{\partial \overline{V}}{\partial \overline{N}} + \frac{R^*\overline{U}}{\overline{N} + R^*}\frac{\partial \overline{V}}{\partial \overline{S}} - \frac{\overline{U}^2}{\overline{N} + R^*}\right] = -\frac{\partial \overline{P}}{\partial \overline{N}} +
$$
$$
\frac{1}{\overline{N} + R^*}\frac{\partial}{\partial \overline{N}}\left((\overline{N} + R^*)\,\overline{\tau}_{\overline{NN}}\right) + \frac{R^*}{\overline{N} + R^*}\frac{\partial}{\partial \overline{S}}\left(\overline{\tau}_{\overline{NS}}\right)
$$
$$
- \frac{\overline{\tau}_{\overline{SS}}}{\overline{N} + R^*} - \frac{\mu}{k_1}\overline{V}, \tag{7}
$$

$$
\rho_f\left[\frac{\partial \overline{U}}{\partial \overline{t}} + \overline{V}\frac{\partial \overline{V}}{\partial \overline{N}} + \frac{R^*\overline{U}}{\overline{N} + R^*}\frac{\partial \overline{U}}{\partial \overline{S}} - \frac{\overline{U}\,\overline{V}}{\overline{N} + R^*}\right]
$$
$$
= -\left(\frac{R^*}{\overline{N} + R^*}\right)\frac{\partial \overline{P}}{\partial \overline{S}} +
$$
$$
\frac{1}{(\overline{N} + R^*)^2}\frac{\partial}{\partial \overline{N}}\left((\overline{N} + R^*)^2\,\overline{\tau}_{\overline{NS}}\right)
$$
$$
+ \frac{R^*}{\overline{N} + R^*}\frac{\partial}{\partial \overline{S}}\left(\overline{\tau}_{\overline{SS}}\right) - \frac{\sigma B_o^2\overline{U}}{(\overline{N} + R^*)^2} - \frac{\mu}{k_1}\overline{U}, \tag{8}
$$

where σ and k_1 are identifying the current density and porosity measures, correspondingly. In the wave frame [36], Eqs. (7) and (8) hold the subsequent form

$$
\rho\left[-c\frac{\partial \overline{v}}{\partial \overline{s}} + \overline{v}\frac{\partial \overline{v}}{\partial \overline{n}} + \frac{R^*(\overline{u} + c)}{\overline{n} + R^*}\frac{\partial \overline{v}}{\partial \overline{s}} - \frac{(\overline{u} + c)^2}{\overline{n} + R^*}\right] = -\frac{\partial \overline{p}}{\partial \overline{n}} +
$$
$$
\frac{1}{\overline{n} + R^*}\frac{\partial}{\partial \overline{n}}\left((\overline{n} + R^*)\,\overline{\tau}_{\overline{nn}}\right) + \frac{R^*}{\overline{n} + R^*}\frac{\partial \overline{\tau}_{\overline{ns}}}{\partial \overline{s}}
$$
$$
- \frac{\overline{\tau}_{\overline{ss}}}{\overline{n} + R^*} - \frac{\mu}{k_1}\overline{v}, \tag{9}
$$

$$\rho_f \left[-c\frac{\partial \overline{u}}{\partial \overline{s}} + \overline{v}\frac{\partial \overline{u}}{\partial \overline{n}} + \frac{R^*(\overline{u}+c)}{\overline{n}+R^*}\frac{\partial \overline{u}}{\partial \overline{s}} + \frac{(\overline{u}+c)\overline{v}}{\overline{n}+R^*} \right]$$

$$= \left(\frac{R^*}{\overline{n}+R^*} \right)\frac{\partial \overline{p}}{\partial \overline{s}} +)$$

$$\frac{1}{(\overline{n}+R^*)^2}\frac{\partial}{\partial \overline{n}}\left\{ (\overline{n}+R^*)\,\overline{\tau}_{\overline{ns}} \right\} + \frac{R^*}{\overline{n}+R^*}\frac{\partial \overline{\tau}_{\overline{ss}}}{\partial \overline{s}}$$

$$- \frac{\sigma B_\circ^2(\overline{u}+c)}{(\overline{n}+R^*)^2} - \frac{\mu}{k_1}(\overline{u}+c) \Bigg). \qquad (10)$$

Now, we make the above equations non-dimensional by incorporating the following dimensionless quantities:

$$s = \frac{2\pi}{\lambda}\overline{s},\ n=\frac{\overline{n}}{a},\ u=\frac{\overline{u}}{c},\ v=\frac{\overline{v}}{c},$$

$$k = \frac{R^*}{a},\ \tau=\frac{a}{\mu c}\overline{\tau},\ Re=\frac{\rho ca}{\mu},\ \varepsilon=\frac{b}{a},$$

$$\delta = \frac{2\pi a}{\lambda},\ p=\frac{2\pi a^2}{\lambda\mu c}\overline{p},\ \beta=\frac{\alpha\mu^2 c^2}{a^2},$$

$$h_1 = \frac{\overline{H}_1}{a},\ h_2=\frac{\overline{H}_2}{a},\ H^2=\frac{\sigma B_0^2 a^2}{\mu},\ Da=\frac{k_1}{a^2}.$$

After imposing above transformations, we found the dimensionless form of Eqs. (9) and (10) which can be observed

$$\delta Re \left[-\delta\frac{\partial v}{\partial s} + v\frac{\partial v}{\partial n} + \delta\frac{k(u+1)}{n+k}\frac{\partial v}{\partial s} - \frac{(u+1)^2}{n+k} \right]$$

$$= -\frac{\partial p}{\partial n} + \delta\left(\frac{1}{n+k}\frac{\partial}{\partial n}\left((n+k)\,\tau_{nn}\right) \right.$$

$$\left. + \delta\frac{k}{n+k}\frac{\partial\tau_{ns}}{\partial s} - \frac{\tau_{ss}}{n+k} - \frac{v}{Da} \right), \qquad (11)$$

$$Re \left[-\delta\frac{\partial u}{\partial s} + v\frac{\partial u}{\partial n} + \delta\frac{k(u+1)}{n+k}\frac{\partial u}{\partial s} - \frac{(u+1)v}{n+k} \right]$$

$$= -\left(\frac{k}{n+k} \right)\frac{\partial p}{\partial s} +)$$

$$\frac{1}{(n+k)^2}\frac{\partial}{\partial n}\left((n+k)^2\,\tau_{ns}\right) + \delta\frac{k}{n+k}\frac{\partial\tau_{ss}}{\partial s}$$

$$- \frac{H^2}{(n+k)^2}(u+1) - \frac{(u+1)}{Da}. \qquad (12)$$

At this stage, we assume the lubrication approach due to waves having small wave number $\delta \to 0$ and negligible effects of turbulence, i.e., $Re \to 0$, and we finally receive

$$\frac{\partial p}{\partial n} = 0 \qquad (13)$$

$$-\left(\frac{k}{n+k} \right)\frac{\partial p}{\partial s} + \frac{1}{(n+k)^2}\frac{\partial}{\partial n}\left((n+k)^2\,\tau_{ns}\right)$$

$$- \frac{H^2}{(n+k)^2}(u+1) - \frac{(u+1)}{Da} = 0, \qquad (14)$$

where the stress component τ_{ns} for Rabinowitsch model is calculated as [36]

$$\tau_{ns} + \beta\tau_{ns}^3 = \frac{\partial u}{\partial n} - \frac{u+1}{n+k} \qquad (15)$$

along with the set of no-slip boundary conditions defined as [33–36]

$$u = -1\ \text{at}\ n = \pm h(s) = \pm\left[1+\varepsilon\cos(s)\right]. \qquad (16)$$

3 Solution procedure

The above achieved relations are coupled non-homogeneous differential equations with variable coefficients. Such complicated equations cannot be tackled by some exact mathematical technique. Hence, we have utilized the combined techniques of perturbation method and HPM [41] to have the series solution which is detailed as below. Let we suggest the following series for τ_{ns} and u by assuming β a small parameter:

$$\tau_{ns} = \tau_{0ns} + \beta\tau_{1ns} + \dots \qquad (17)$$
$$u = u_0 + \beta u_1 + \dots \qquad (18)$$

Using above series in (14) and (15) and equating the terms of zeroth and first exponents of β, we achieve the following two systems.

Coefficients of β^0:

$$-\left(\frac{k}{n+k} \right)\frac{\partial p}{\partial s} + \frac{1}{(n+k)^2}\frac{\partial}{\partial n}\left((n+k)^2\,\tau_{0ns}\right)$$

$$- \frac{H^2}{(n+k)^2}(u_0+1) - \frac{(u_0+1)}{Da} = 0, \qquad (19)$$

$$\tau_{0ns} = \frac{\partial u_0}{\partial n} - \frac{(u_0+1)}{n+k}. \qquad (20)$$

Putting Eq. (20) in Eq. (19), we approach

$$-\left(\frac{k}{n+k} \right)\frac{\partial p}{\partial s} + \frac{1}{(n+k)^2}\frac{\partial}{\partial n}$$

$$\left[(n+k)^2\left(\frac{\partial u_0}{\partial n} - \frac{(u_0+1)}{n+k} \right) \right]$$

$$- \frac{H^2}{(n+k)^2}(u_0+1) - \frac{(u_0+1)}{Da} = 0. \Bigg) \qquad (21)$$

with boundary conditions

$$u_0 = -1\ \text{at}\ n = \pm h(s) = \pm\left[1+\varepsilon\cos(s)\right]. \qquad (22)$$

Coefficients of β:

$$\frac{1}{(n+k)^2}\frac{\partial}{\partial n}\left((n+k)^2\,\tau_{1ns}\right)$$

$$-\frac{H^2}{(n+k)^2}u_1 - \frac{u_1}{Da} = 0, \qquad (23)$$

$$\tau_{1ns} + \tau_{0ns}^3 = \frac{\partial u_1}{\partial n} - \frac{u_1}{n+k} \qquad (24)$$

or

$$\tau_{1ns} = \frac{\partial u_1}{\partial n} - \frac{u_1}{n+k} - \left[\left(\frac{\partial u_0}{\partial n} - \frac{(u_0+1)}{n+k}\right)\right]^3. \qquad (25)$$

Putting Eq. (25) in Eq. (23)

$$\frac{1}{(n+k)^2}\frac{\partial}{\partial n}\left[(n+k)^2\left(\frac{\partial u_1}{\partial n} - \frac{u_1}{n+k} - \left(\frac{\partial u_0}{\partial n}\right.\right.\right.$$
$$\left.\left.\left.-\frac{(u_0+1)}{n+k}\right)^3\right)\right]$$
$$\left.-\frac{H^2}{(n+k)^2}u_1 - \frac{u_1}{Da} = 0\right), \qquad (26)$$

and boundary conditions are

$$u_1 = 0 \text{ at } n = \pm h(s). \qquad (27)$$

Solution of u_0 by HPM

Now, we use HPM to solve the above obtained highly complicated systems of differential equations.

Let us find the solution of zeroth order system. As per policy of HPM, we first construct the deformation relation for u_0 as follows:

$$\mathcal{D}\left[u_0 - \widehat{u_0}\right] + q\left[\widehat{N}(u_0)\right] = 0, \qquad (28)$$

where $\mathcal{D}$ is the linear differential operator of our own choice keeping in mind the order of differential equation and is selected as $\mathcal{D} = \frac{\partial^2}{\partial n^2}$, q is embedding parameter, and $\widehat{N}$ stands for the given operator applied on the unknown variable along with forcing functions of independent variable. Equation (26) takes the following form:

$$\frac{\partial^2}{\partial n^2}[u_0-] + q\left[-\left(\frac{k}{n+k}\right)\frac{\partial p}{\partial s}\right.$$
$$+\frac{1}{(n+k)^2}\frac{\partial}{\partial n}\left((n+k)^2\left(\frac{\partial u_0}{\partial n} - \frac{(u_0+1)}{n+k}\right)\right)$$
$$\left.-\frac{H^2}{(n+k)^2}(u_0+1) - \frac{(u_0+1)}{Da}\right] = 0. \Bigg) \qquad (29)$$

Moreover, $_0$ is an initial guess and it is suggested as

$$\widehat{u} = \frac{-2Da - h^2 + n^2}{2Da}. \qquad (30)$$

Now, we take the series expansion of u_0 as increasing exponents of q, that is

$$u_0 = u_{01} + qu_{02} + \dots \qquad (31)$$

Zeroth-order system for u_0

Equating the coefficients of q^0, we observe the following system with corresponding conditions defined on the walls:

$$\mathcal{D}\left[u_{01} - \widehat{u_0}\right] = 0, \qquad (32)$$
$$u_{01} = -1 \text{ at } n = \pm h(s). \qquad (33)$$

First-order system for u_0

Equating the coefficients of q, we extract the another system of equations with respective surface conditions and is elaborated as

$$\mathcal{D}[u_{02}] + \frac{\partial^2 u_{01}}{\partial n^2}$$
$$+\frac{2}{n+k}\frac{\partial u_{01}}{\partial n} + \frac{1}{(n+k)^2}\frac{\partial}{\partial n}((n+k)(u_0+1))$$
$$-\left(\frac{k}{n+k}\right)\frac{\partial p}{\partial s} = 0. \qquad (34)$$
$$u_{02} = 0 \text{ at } n = \pm h(s). \qquad (35)$$

After solving above two systems, we get

$$u_{01} = \widehat{u} = \frac{(-2Da - h^2 + n^2)}{2Da} \qquad (36)$$

and

$$u_{02} = -\frac{1}{12Da^2 h(k+n)}$$
$$\begin{pmatrix} h(h-n)(h+n)(3Da(-3+H^2)k - 9Dan \\ -k(3k-n)(k+n) + 6Da^2(k+n)p) \\ +3(k+n)(((h-k)^2k(h+k) \\ +Da(h^2 - hH^2k + (-1+3H^2)k^2)) \\ (h-n)Log[-h+k] + (-(h-k)k(h+k)^2 \\ +D^2h^2 + hH^2k + (-1+3H^2)k^2)) \\ (h+n)Log[h+k] - 2h(k(-h^2+k^2) \\ (k+n) + Da(h^2 + k(-k+3H^2k+H^2n))) \\ Log[k+n]) \end{pmatrix} \qquad (37)$$

Solution of u_1 by HPM

Let us define the homotopy equation for u_1 as

$$\mathcal{D}\left[u_1 - \widehat{u_1}\right] + q\left[\widehat{N}(u_1)\right] = 0, \qquad (38)$$

where $\widehat{u_1}$ is an initial guess which is chosen as

$$\widehat{u_1} = \frac{(-h^2 + n^2)}{2Da}. \qquad (39)$$

Equation (38) can be replaced by the following form:

550

Eur. Phys. J. Spec. Top. (2022) 231:545–555

Table 1 Validation of the current results by comparing with the existing literature [36]

Variation of curvature parameter k	Stress tensor Data in study [36]	Current Stress tensor data with Da = 100 and Ha = 0	Current Stress tensor data with Da = 2.5 and H = 1.5
1.10	1.51009	1.51023	-0.12987
1.15	1.51075	1.51081	0.25192
1.20	1.51118	1.51120	0.509586
1.25	1.51148	1.51151	0.694366
1.30	1.51169	1.51172	0.832676
1.35	1.51185	1.51191	0.939529
1.40	1.51196	1.51102	1.02411
1.45	1.51204	1.51215	1.09236
1.50	1.51209	1.51211	1.14832

$$\frac{\partial^2}{\partial n^2}\left[u_1-\right] + q\left[\frac{1}{(n+k)^2}\frac{\partial}{\partial n}\left\{(n+k)^2\left(\frac{\partial u_1}{\partial n}\right.\right.\right.$$
$$\left.\left.\left.-\frac{u_1}{n+k}-\left(\frac{\partial u_0}{\partial n}-\frac{(u_0+1)}{n+k}\right)^3\right)\right\}\right.$$
$$\left.-\frac{H^2}{(n+k)^2}u_1-\frac{u_1}{Da}\right] = 0\Bigg). \tag{40}$$

Let us suppose

$$u_1 = u_{11} + q u_{12}\dots \tag{41}$$

Inserting the above series of u_1 into Eq. (40), we can build the two systems by equating coefficients of q.

Zeroth-order system for u_1

$$\mathcal{D}\left[u_{11}-\widehat{u_1}\right] = 0, \tag{42}$$

with boundary conditions

$$u_{11}\left[\pm h(s)\right] = 0. \tag{43}$$

First-order system for u_1

$$D\left[u_{12}\right] + \frac{1}{(n+k)^2}\frac{\partial}{\partial n}\left[(n+k)^2\left(\frac{\partial u_{11}}{\partial n}\right.\right.$$
$$\left.\left.-\frac{u_{11}}{n+k}-\left(\frac{\partial u_{01}}{\partial n}-\frac{(u_{01}+1)}{n+k}\right)^3\right)\right]$$
$$-\frac{H^2}{(n+k)^2}u_{11}-\frac{u_{11}}{Da} = 0, \tag{44}$$

with

$$u_{12}\left[\pm h(s)\right] = 0. \tag{45}$$

After solving above equations simultaneously, we gather

$$u_{11} = \widehat{u_1} = \frac{(-h^2+n^2)}{2Da}, \tag{46}$$

$$u_{12} = \frac{1}{96Da^3 hk(k+n)}$$
$$\begin{pmatrix}
(h(h-n)(h+n)(6h^4+342k^4+228k^3n\\
-81k^2n^2-54kn^3-81n^4-24Da^2\\
((-3+H^2)k-n)(k+n)-4Dakn^2(k+n)\\
+h^2((-363+20Da)k^2+10(-27+2Da)kn\\
+81n^2))+6(k+n)((h-k)(9h^4\\
-66h^2k^2+57k^4-4Da^2(h^2+hH^2k\\
+(-1+3H^2)k^2))(h-n)Log[-h+k]\\
+(h+k)(-9h^4+66h^2k^2-57k^4\\
+4Da^2(h^2-hH^2k+(-1+3H^2)k^2))(h+n))\\
Log[h+k]+2h(3(3h^4-22h^2k^2+19k^4)\\
(k+n)+4Da^2(h^2((-1+H^2)k-n)\\
+k^2(k-3H^2k+n-2H^2n)))Log[k+n]))
\end{pmatrix}. \tag{47}$$

The pressure gradient dp/dx can be evaluated as

$$\frac{dp}{dx} = \frac{1}{2h^3}$$
$$\left(3\begin{pmatrix}
-2h-Q-\frac{h(87h^4-190h^2k^2+105k^4)\beta}{15Da^3}\\
+\frac{h(25h^2k^2-15k^4+8h^4\beta)}{30Da^2}\\
-\frac{h(3k^2(-2+H^2(6-4\beta)+\beta)+h^2(4+(-5+8H^2)\beta))}{6Da}\\
-\frac{1}{4Da^3k}\begin{pmatrix}
Da(-h^2k+k^3)^2-2(h^2-7k^2)\\
(h^2-k^2)^2\beta+Da^2(h^4\beta+k^4\\
(-2+H^2(6-4\beta)+\beta+2h^2k^2\\
(1-\beta+H^2(-1+2\beta))))\\
(Log[-h+k]-Log[h+k])
\end{pmatrix}
\end{pmatrix}\right). \tag{48}$$

4 Graphical results and discussion

This section is included to examine the tabular and graphical results of involved parameters affecting the flow characteristics. To relate the current investigation with existing literature and to enhance the validity graph of the current study, we have presented a Table 1 which clearly indicates that the study published in [36] is a limiting case of the current analysis when we overlook the effects of porosity and magnetic features. To observe the influence of emerging parameters, we have
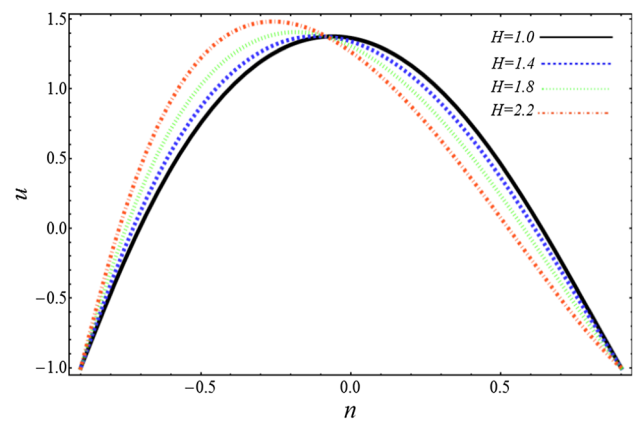
Eur. Phys. J. Spec. Top. (2022) 231:545–555

551
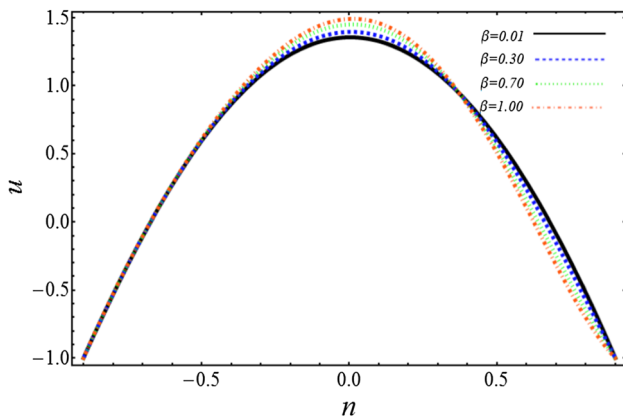
Fig. 2 Alteration of velocity field u for β along with $k = 2, s = \pi, Q = 1, \varepsilon = 0.1, Da = 0.6, H = 1$
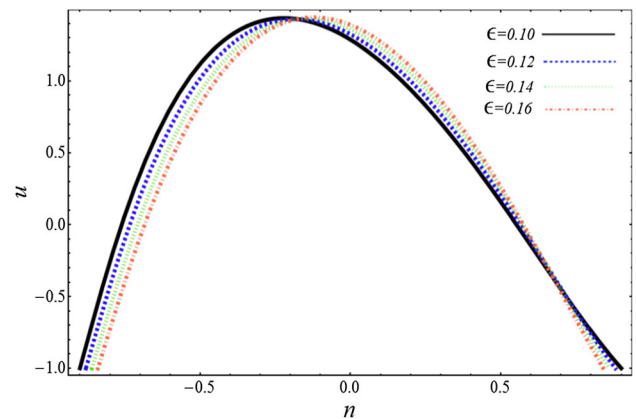
Fig. 4 Alteration of velocity field u for ε along with $k = 1.2, s = \pi, Q = 1, \beta = 0.05, Da = 0.4, H = 2$
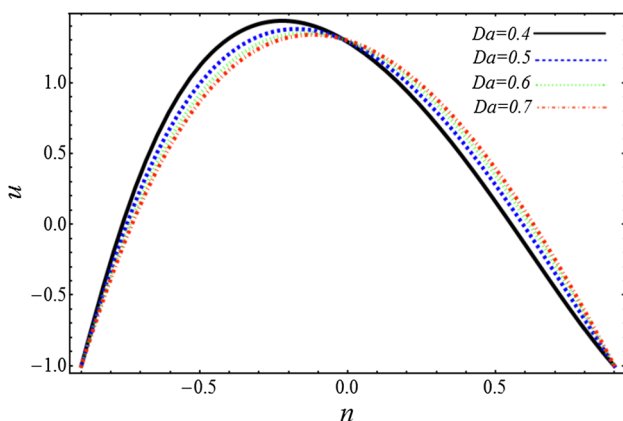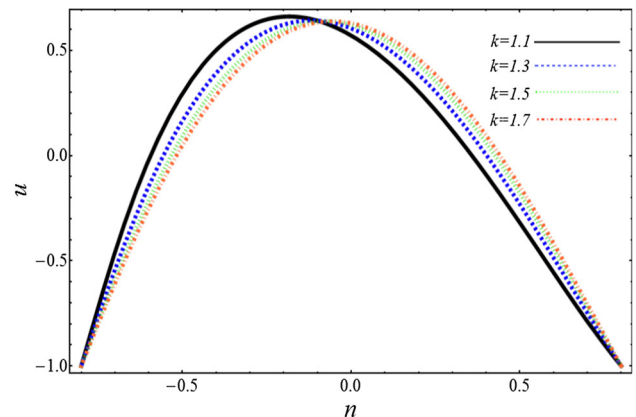

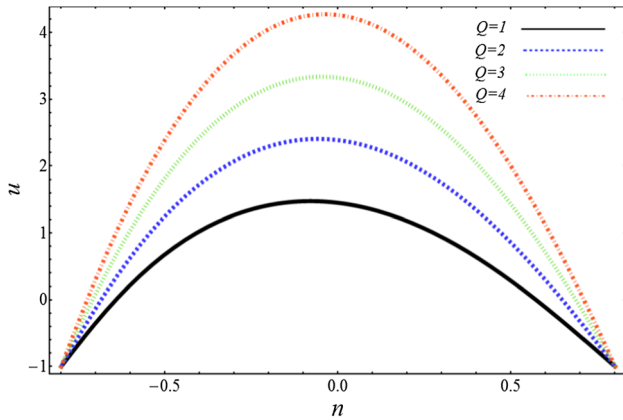**Fig. 3** Alteration of velocity field u for Da along with $k = 1.2, s = \pi Q = 1, \varepsilon = 0.1, \beta = 0.05, H = 2$

Fig. 5 Alteration of velocity field u for H along with $k = 1.2, s = \pi, Q = 1, \varepsilon = 0.1, Da = 0.4, \beta = 0.05$

Fig. 6 Alteration of velocity field u for k along with $\beta = 0.05, s = \pi, Q = 0.1, \varepsilon = 0.2, Da = 0.4, H = 2$

portrayed the Figs. 2, 3, 4, 5, 6, 7, 8, 9, 10, 11,12 13. Figures (2, 3, 4, 5, 6, 7) contain the graphs of velocity components u drawn against the radial factor n under the alteration of fluid parameter β, Darcy number Da, the amplitude ratio ε, Hartman number H, curvature k, and flow rate Q, respectively. Figures 8, 9, 10, 11 reveal the characteristics of pressure gradient curves against the β, Da, H, and K, correspondingly. We can observe the trapping analysis from Figs. 12 and 13 which are sketched under the variation of Da and H.

From Fig. 2, we can extract that velocity is varying directly with the increasing effect of β in left and middle parts of the channel, but the curves are declined in the right side. This can physically explain that the magnitude of β represents the elasticity of the fluid which rapids up the fluid accordingly. Figure 3 implies that velocity is lowering in the domain $[-h, 0)$ but rising in $(0, h]$ by ascending variations of Da. It reflects the physical reasoning that porosity of the medium affects the flow in lower and central regions of the channel significantly as compared to the upper half. The behavior of velocity projectile under the increments of amplitude ratio ε is quite similar to that of porosity parameter Da. It is noted from Fig 5 that Hartmann number makes
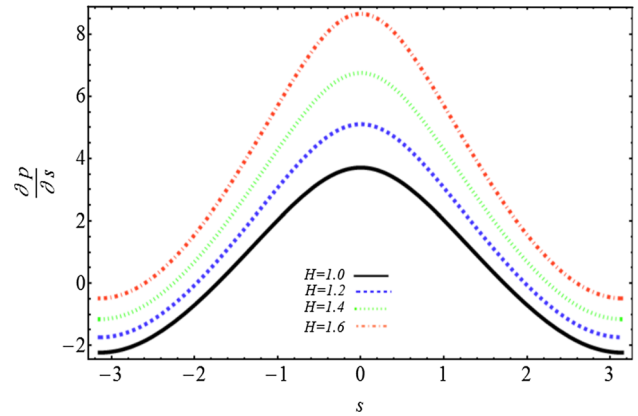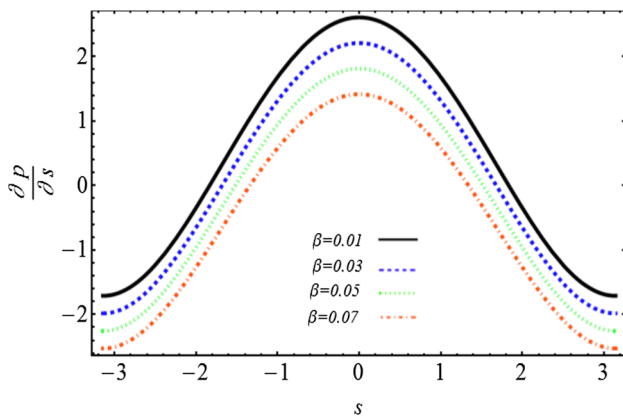
the flow faster in lower area and gives reflexive behavior in the upper portion. This result is quite against the consequences found for Darcy number. It may be due to the fact that the magnetic field is applied in transverse direction to the flow which has suppressed the flow more comprehensively in the upper arrear as compared to the
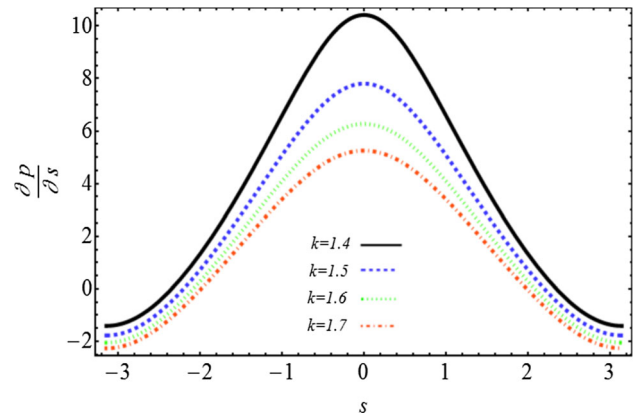
Fig. 7 Alteration of velocity field u for Q along with $k = 1.2, s = \pi, \beta = 0.05, \varepsilon = 0.2, Da = 0.4, H = 2$

Fig. 8 Alteration of pressure $\frac{\partial p}{\partial s}$ for β along with $k = 2, Q = 1, \varepsilon = 0.1, Da = 0.3, H = 1$

Fig. 9 Alteration of pressure $\frac{\partial p}{\partial s}$ for Da along with $k = 1.2, Q = 1, \varepsilon = 0.1, \beta = 0.05, H = 2$

far away region. The readings of k on velocity profile are almost in line with that of received for Darcy number Da (Fig. 6). It means that porosity, curvature of channel, and amplitude ratio affect the flow in quite same manner. It is assumed from Fig. 7 that when we larger the numerical values of flow rate Q, the velocity increases throughout the channel. It reflects that
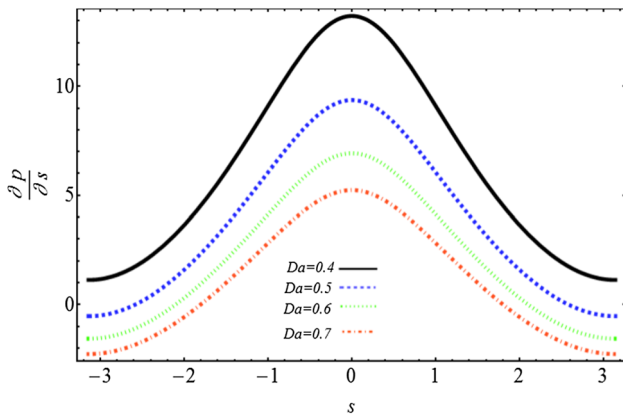

Fig. 10 Alteration of pressure $\frac{\partial p}{\partial s}$ for H along with $k = 1.2, Q = 1, \varepsilon = 0.1, \beta = 0.05, Da = 0.4$

Fig. 11 Alteration of pressure $\frac{\partial p}{\partial s}$ for k along with $Da = 0.4, Q = 0.1, \varepsilon = 0.2, \beta = 0.05, H = 2$

fluid travels fast if the amount of fluid per unit time is enhanced.

Figures 8, 9, 10, 11 comprise the plot of pressure gradient profile $\frac{\partial p}{\partial s}$ drawn against the flow rate Q for parameters β, Da, H, and k, correspondingly. From Fig. 8, it is concluded that $\frac{\partial p}{\partial s}$ is decreasing with the large values of β and it becomes maximum at the center as compared the corners of the channels. This is because in the middle part of the channel, a more pressure gradient is required to maintain the flow rate, but the elasticity of the fluid decreases its magnitude. The effect of the porosity representative Da is almost same as we have examined for β (see Fig. 9), but in this diagram, the height of the curves is getting higher than the previous ones. It is measured from Fig. 10 that pressure gradient is getting large with the variation of applied magnetic field. Physically, it suggests that the fluid is traveling faster as observed above which may be the cause of increase in pressure profile to settle down the flow rate. The pressure curves for k can be visualized in Fig 11 and it is easily found here that $\frac{\partial p}{\partial s}$ is diminishing its height when
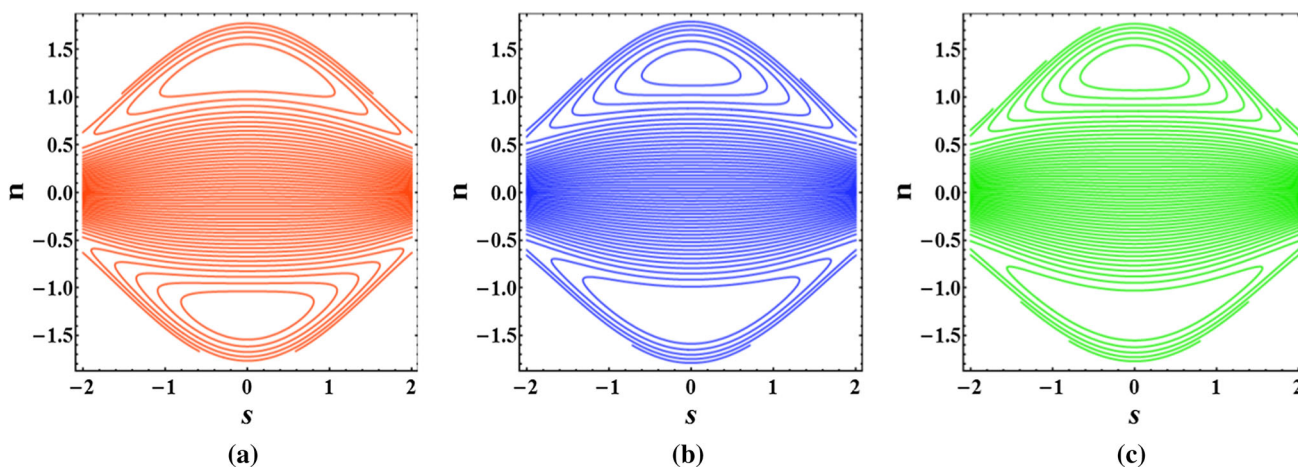
Eur. Phys. J. Spec. Top. (2022) 231:545–555

553

Fig. 12 Streamline for Da (a) for $Da = 5$, (b) for $Da = 5.5$, (c) for $Da = 6$
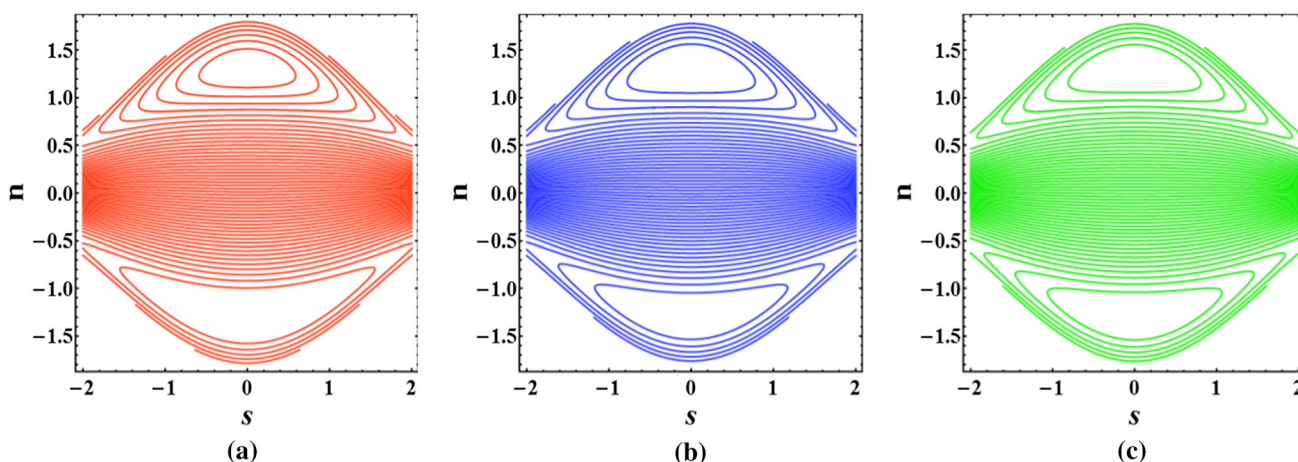

Fig. 13 Streamline for H (a) for $H = 0.1$, (b) for $H = 0.2$, (c) for $H = 0.3$

we give large magnitude to the curvature parameter k
.

Figures 12 and 13 suggest the scene of flow pattern for different parameters. These graphs contain the contours of stream function ψ plotted in two-dimensional domains. Figure 12 contains the streamlines of the parameters Da; it can be obtained here that a circulating bolus is becoming large in lower part but shorter its size in upper part of the container with increasing values of Da. It can also be seen that the flow is symmetric about the center line which is also depicting the assumption symmetric channel. It can be noticed from Fig. 13 that totally opposite scenario is observed in the sketch of streamlines for the MHD parameter H. It shows that porous medium and MHD are exerting quite different impact on flow pattern.

5 Conclusions

In this communication, we have analyzed the theoretical study of pumping characteristics of the same fluid with same circumstances along with the inclusion of two new factors, the porous medium and the MHD. After getting the analytic solution, we have seen the graphical picture of whole the analysis. The key points which we have achieved are manipulated as:

Porous medium is restricting the flow velocity in lower part of the channel, but in upper side, there is no hindrance to the flow.
It is found that the magnetic field opposes the flow speed in half side, but increases it in other region.
It is concluded that peristaltic pressure is increased with magnetic field, but decreased with porosity factor.
It is also evident from above analysis that flow pattern is showing totally opposite picture for porosity and MHD.
It is also measured that the current study gives the data of [36] as a limiting case of H=0 and Da=infinity.

554

Eur. Phys. J. Spec. Top. (2022) 231:545–555

References

1. A. Riaz, A. Razaq, A.U. Awan, Magnetic field and permeability effects on Jeffrey fluid in eccentric tubes having flexible porous boundaries. Journal of Magnetics **22**(4), 642–648 (2017)

2. S. Noreen, Induced Magnetic Field Effects on Peristaltic Flow in a Curved Channel. ZeitschriftfürNaturforschung A, **70**(1), 3-9 (2015)

3. A. Riaz, A. Zeeshan, S. Ahmad, A. Razaq, M. Zubair, Effects of external magnetic field on Non-newtonian two phase fluid in an annulus with peristaltic pumping. Journal of Magnetics **24**(1), 62–69 (2019)

4. A. Zeeshan, N. Ijaz, M.M. Bhatti, Flow analysis of particulate suspension on an asymmetric peristaltic motion in a curved configuration with heat and mass transfer. Mechanics & Industry **19**(4), 401 (2018)

5. S. Srinivas, M. Kothandapani, The influence of heat and mass transfer on MHD peristaltic flow through a porous space with compliant walls. Applied Mathematics and Computation **213**(1), 197–208 (2009)

6. E.N. Maraj, N.S. Akbar, N. Nadeem, Mathematical study for peristaltic flow of Williamson fluid in a curved channel. International Journal of Biomathematics **8**(1), 1550005 (2015)

7. N.S. Akbar, A.W. Butt, Carbon nanotubes analysis for the peristaltic flow in curved channel with heat transfer. Applied Mathematics and Computation **259**, 231–241 (2015)

8. H. Shamsabadi, S. Rashidi, J.A. Esfahani, Entropy generation analysis for nanofluid flow inside a duct equipped with porous baffles. Journal of Thermal Analysis and Calorimetry **135**, 1009–1019 (2019)

9. R. Alizadeh, N. Karimi, R. Arjmandzadeh, A. Mehdizadeh, Mixed convection and thermodynamic irreversibilities in MHD nanofluid stagnation-point flows over a cylinder embedded in porous media. Journal of Thermal Analysis and Calorimetry **135**, 489–506 (2019)

10. T. Hayat, B. Ahmed, F.M. Abbasi, A. Alsaedi, Numerical investigation for peristaltic flow of Carreau-Yasuda magneto-nanofluid with modified Darcy and radiation. Journal of Thermal Analysis and Calorimetry **135**, 1359–1367 (2019)

11. J. Stiller, K. Koal, W.E. Nagel, J. Pal, A. Cramer, Liquid metal flows driven by rotating and traveling magnetic fields. The European Physical Journal Special Topics **220**(1), 111–122 (2013)

12. G. Sucharitha, K. Vajravelu, P. Lakshminarayana, Effect of heat and mass transfer on the peristaltic flow of a Jeffrey nanofluid in a tapered flexible channel in the presence of aligned magnetic field. The European Physical Journal Special Topics **228**(12), 2713–2728 (2019)

13. R. Meenakumari, P. Lakshminarayana, K. Vajravelu, Unsteady MHD flow of a Williamson nanofluid on a permeable stretching surface with radiation and chemical reaction effects. The European Physical Journal Special Topics, 1-16 (2021)

14. S. P. Samrat, M.G. Reddy, N. Sandeep, Buoyancy effect on magnetohydrodynamic radiative flow of Casson fluid with Brownian moment and thermophoresis. The European Physical Journal Special Topics, 1-9 (2021)

15. M. Trivedi, M.S. Ansari, Unsteady Casson fluid flow in a porous medium with inclined magnetic field in presence of nanoparticles. The European Physical Journal Special Topics **228**(12), 2553–2569 (2019)

16. M.I. Khan, Y.M. Chu, F. Alzahrani, A. Hobiny, Comparative analysis of Al2O3-47 nm and Al2O3-36 nm hybrid nanoparticles in a symmetric porous peristaltic channel. Physica Scripta **96**(5), 055005 (2021)

17. N. Khan, M. Riaz, M.S. Hashmi, S.U. Khan, I. Tlili, M.I. Khan, M. Nazeer, Soret and Dufour features in peristaltic motion of chemically reactive fluid in a tapered asymmetric channel in the presence of Hall current. Journal of Physics Communications **4**(9), 095009 (2020)

18. S. Farooq, M.I. Khan, M. Waqas, T. Hayat, A. Alsaedi, Transport of hybrid type nanomaterials in peristaltic activity of viscous fluid considering nonlinear radiation, entropy optimization and slip effects. Computer Methods and Programs in Biomedicine. **184**, 105086 (2020)

19. V.K. Narla, D. Tripathi, O.A. Bég, A. Kadir, Modeling transient magnetohydrodynamic peristaltic pumping of electroconductive viscoelastic fluids through a deformable curved channel. Journal of Engineering Mathematics **111**(1), 127–143 (2018)

20. M. Qasim, Z. Ali, A. Wakif, Z. Boulahia, Numerical simulation of MHD peristaltic flow with variable electrical conductivity and Joule dissipation using generalized differential quadrature method. Communications in Theoretical Physics **71**(5), 509 (2019)

21. C.H. Amanulla, A. Wakif, Z. Boulahia, M.S. Reddy, N. Nagendra, Numerical investigations on magnetic field modeling for Carreau non-Newtonian fluid flow past an isothermal sphere. Journal of the Brazilian Society of Mechanical Sciences and Engineering **40**(9), 462 (2018)

22. S. E. Ahmed, Z. A. Raizah, A. M. Aly, Three-dimensional flow of a power-law nanofluid within a cubic domain filled with a heat-generating and 3D-heterogeneous porous medium. The European Physical Journal Special Topics, 1-15 (2021)

23. R. N. Kumar, R. P. Gowda, B. J. Gireesha, B. C. Prasannakumara, Non-Newtonian hybrid nanofluid flow over vertically upward/downward moving rotating disk in a Darcy–Forchheimer porous medium. The European Physical Journal Special Topics, 1-11 (2021)

24. A. Jarray, Z. Mehrez, A. El Cafsi, Mixed convection agmgo/water hybrid nanofluid flow in a porous horizontal channel. The European Physical Journal Special Topics **228**(12), 2677–2693 (2019)

25. T. Hayat, S. Ayub, A. Alsaedi, Homogeneous-heterogeneous reactions in curved channel with porous medium. Results in Physics **9**, 1455–1461 (2018)

26. S.A. Mohammadein, A.K. Abu-Nab, Peristaltic flow of a newtonian fluid through a porous medium surrounded vapour bubble in a curved channel. Journal of Nanofluids **8**(3), 651–656 (2019)

27. K. Vajravelu, S. Sreenadh, P. Lakshminarayana, G. Sucharitha, M.M. Rashidi, Peristaltic flow of Phan-Thien-Tanner fluid in an asymmetric channel with porous medium. Journal of Applied Fluid Mechanics **9**(4), 1615–1625 (2016)

Eur. Phys. J. Spec. Top. (2022) 231:545–555

555

28. A.M. Abd-Alla, S.M. Abo-Dahab, R.D. Al-Simery, Effect of rotation on peristaltic flow of a micropolar fluid through a porous medium with an external magnetic field. Journal of magnetism and Magnetic materials **348**, 33–43 (2013)

29. M.M. Rashidi, M. Keimanesh, O.A. Bég, T.K. Hung, Magnetohydrodynamicbiorheological transport phenomena in a porous medium: a simulation of magnetic blood flow control and filtration. International Journal for Numerical Methods in Biomedical Engineering **27**(6), 805–821 (2011)

30. M.G. Reddy, Heat and mass transfer on magnetohydrodynamic peristaltic flow in a porous medium with partial slip. Alexandria Engineering Journal **55**(2), 1225–1234 (2016)

31. N.S. Akbar, A.W. Butt, Heat transfer analysis of Rabinowitsch fluid flow due to metachronal wave of cilia. Results in physics **5**, 92–98 (2015)

32. H. Vaidya, C. Rajashekhar, G. Manjunatha, K.V. Prasad, Effect of variable liquid properties on peristaltic flow of a Rabinowitsch fluid in an inclined convective porous channel. The European Physical Journal Plus **134**(5), 231 (2019)

33. H. Vaidya, C. Rajashekhar, G. Manjunatha, K.V. Prasad, Peristaltic mechanism of a Rabinowitsch fluid in an inclined channel with complaint wall and variable liquid properties. Journal of the Brazilian Society of Mechanical Sciences and Engineering **41**(1), 52 (2019)

34. H. Sadaf, S. Nadeem, Analysis of combined convective and viscous dissipation effects for peristaltic flow of Rabinowitsch fluid model. Journal of Bionic Engineering **14**(1), 182–190 (2017)

35. H. Vaidya, C. Rajashekhar, G. Manjunatha, K. V. Prasad, O. D. Makinde, S. Sreenadh, Peristaltic motion of non-Newtonian fluid with variable liquid properties in a convectively heated nonuniform tube: Rabinowitsch fluid model. Journal of Enhanced Heat Transfer, **26**(3) (2019)

36. N. Ali, M. Sajid, K. Javid, R. Ahmed, Peristaltic flow of Rabinowitsch fluid in a curved channel: mathematical analysis revisited. ZeitschriftfürNaturforschung A, **72**(3), 245-251 (2017)

37. U.P. Singh, R.S. Gupta, V.K. Kapur, On the steady performance of annular hydrostatic thrust bearing: Rabinowitsch fluid model. Journal of tribology **134**(4), 044502 (2012)

38. A. K. Rahul, P. S. Rao, Rabinowitsch fluid flow with viscosity variation: Application of porous rough circular stepped plates. Tribology International, 106635 (2020)

39. N. Imran, M. Javed, M. Sohail, S. Farooq, M. Qayyum, Outcome of slip features on the peristaltic flow of a Rabinowitschnanofluid in an asymmetric flexible channel. Multidiscipline Modeling in Materials and Structures (2020)

40. M. Zahid, M. Zafar, M.A. Rana, M.T.A. Rana, M.S. Lodhi, Numerical analysis of the forward roll coating of a rabinowitsch fluid. J. Plast. Film Sheeting **36**, 191–208 (2020)

41. J.H. He, Homotopy perturbation method: a new nonlinear analytical technique. Applied Mathematics and computation **135**(1), 73–79 (2003)